Dynamics of the Preprotein Translocation Channel of the Outer Membrane of Mitochondria

Melissa Poynor, Reiner Eckert, and Stephan Nussberger
Abteilung Biophysik, Biologisches Institut, Universität Stuttgart, Stuttgart, Germany

ABSTRACT The protein translocase of the outer mitochondrial membrane (TOM) serves as the main entry site for virtually all mitochondrial proteins. Like many other protein translocases it also has an ion channel activity that can be used to study the dynamical properties of this supramolecular complex. We have purified TOM core complex and Tom40, the main pore forming subunit, from mitochondria of the filamentous fungus *Neurospora crassa* and incorporated them into planar lipid bilayers. We then examined their single channel properties to provide a detailed description of the conformational dynamics of this channel in the absence of its protein substrate. For isolated TOM core complex we have found at least six conductance states. Transitions between these states were voltage-dependent with a bell-shaped open probability distribution and distinct kinetics depending on the polarity of the applied voltage. The states with the largest conductance followed an Ohmic I/V characteristic consistent with a large cylindrical pore with very little interaction with the permeating ions. For the lower conductance states, however, we have observed inverted *S*-shaped nonlinear current-voltage curves reminiscent to those of much narrower pores where the permeating ions have to surmount an electrostatic energy barrier. At low voltages ($<\pm 70$ mV), purified Tom40 protein did not show any transitions between its conductance states. Prolonged exposure to higher voltages induced similar gating behavior to what we observed for TOM core complex. This effect was time-dependent and reversible, indicating that Tom40 forms not only the pore but also contains the "gating machinery" of the complex. However, for proper functioning, additional proteins (Tom22, Tom7, Tom6, and Tom5) are required that act as a modulator of the pore dynamics by significantly reducing the energy barrier between different conformational states.

INTRODUCTION

The protein translocase of the outer mitochondrial membrane (TOM) represents the main entry site into mitochondria for virtually all mitochondrial precursor proteins. It regulates the interaction of preproteins with the mitochondrion and mediates the transfer of unfolded polypeptides across the outer membrane. In addition, it plays a central role in the integration of membrane proteins into the outer membrane (1–7).

The TOM transferase is a supramolecular complex. The central subunit that forms the protein-conducting channel has been assigned to Tom40 (8–11). TOM core complex includes the preprotein receptor Tom22 and three proteins that function in the assembly and stability of the complex, Tom5, Tom6, and Tom7 (12–18). TOM holo complex also contains Tom20 and Tom70 that interact with the channel at its periphery only and thus play a minor role in channel formation.

Using an electrophysiological approach, Tom40, TOM core complex, and TOM holo complex have been shown to form large ion-conducting channels in lipid membranes (8–11,19). This channel activity closely resembles channels found in native mitochondrial membranes. The so-called peptide sensitive channels, PSC, are slightly cation selective and are blocked by preprotein peptides (20–24). These PSC channels have subsequently shown to be identical with the TOM-translocase (25,26). Like other protein translocases, the TOM channel was found to have a considerably large conductivity and a pore size of ~2 nm (27–33). Using outer mitochondrial membranes of *Saccharomyces cerevisiae* wild-type and tom22Δ deletion mutants it has also been suggested that the preprotein receptor Tom22 plays an essential role in regulating the channel activity of the TOM complex (16).

At high membrane voltages, the TOM channels were found to undergo fast transitions between multiple conductance states, particularly from a maximum open state to two nearly equidistant lower conductance states (10,11,26,30, 34). Based on this observation and low resolution electron microscopy studies, the TOM core complex has been proposed to form a ''double-barreled'' channel in the outer membrane of mitochondria (5).

Although the importance of the TOM complex in the mitochondrial protein translocation pathway is well established, little is known about the biophysical mechanism of protein binding and translocation. The current working hypothesis is that TOM forms an aqueous pore through which polypeptides thread across the mitochondrial outer membrane. It is believed that this pore is identical with the ion conducting pathway. If this is the case then each transition of a substrate peptide would block the pore for ion passage and electrophysiological data could be described in terms of a Woodhull blocking mechanism (35,36).

Submitted February 6, 2008, and accepted for publication April 7, 2008.

Address reprint requests to Stephan Nussberger, Abteilung Biophysik, Biologisches Institut, Universität Stuttgart, Pfaffenwaldring 57, D-70550 Stuttgart, Germany. Tel.: 49-711-6856-5002; Fax: 49-711-6856-5090; E-mail: nussberger@bio.uni-stuttgart.de.

Editor: Richard W. Aldrich.

0006-3495/08/08/1511/12 $2.00

doi: 10.1529/biophysj.108.131003

So far, the transfer of polymers has been studied with model pores, like α-hemolysin and macromolecules such as oligonucleotides (37–40), peptides (41), or polysugars (42). Substrate–pore interactions and partitioning of substrate into individual pores were explored by probing the frequency and duration of transient substrate-induced current blockages. Current blockages were found to be sensitive to the properties of the biopolymers and provided a rich source of information to elucidate the mechanism of polymer capture and transport on physical grounds (43).

In contrast to α-hemolysin, TOM shows spontaneous voltage-dependent gating behavior. Therefore, to adopt a similar experimental approach to TOM and gain information regarding the dynamics of polypeptides in the TOM-channel, the detection of substrate-induced current blockages requires detailed knowledge of the kinetic behavior of the TOM channels in the absence and presence of substrate peptides. Although there is a large body of electrophysiological data available, a comprehensive characterization of TOM as a gated ion channel has still been lacking.

In this study, we have examined the single channel properties of TOM isolated from *Neurospora crassa* to provide a detailed description of the conformational dynamics of the TOM complex pore in the absence of blocking peptide substrate. We describe a kinetic model of the channel activity that can be used to identify substrate-induced current blockages among the intrinsic gating of the TOM machinery. The model will also help to decide which of the substates are affected by peptide blockage and represent peptide transporting configurations.

MATERIALS AND METHODS

Isolation of TOM core complex

TOM core complex was purified from *N. crassa* strain GR-107 that contains a hexahistidinyl-tagged form of Tom22. Protein was isolated from detergent solubilized mitochondria according to the protocol of (44) by nickel-nitrilotriacetic acid affinity (Ni-NTA) and anion exchange chromatography with minor modifications regarding the buffer (20 mM Tris, pH 8.5) for the first isolation steps.

TOM core complex lacking either subunit Tom5, Tom6, or Tom7 was purified from *N. crassa* strains *tom5RIP*, *tom6RIP*, and *tom7KO-35* (13,18). Purified mitochondrial outer membranes (26) were solubilized in 1% *n*-dodecyl β-D-maltoside (DDM), 20% glycerol, 50 mM K-acetate, 10 mM Mops (pH 7.2), and 1 mM phenylmethylsulfonyl fluoride (PMSF) at 4°C for 30 min. After removal of insoluble material by centrifugation at 130,000 $\times$ *g*, the soluble extract was bound to an anion exchange Resource Q column (GE Healthcare, Munich, Germany). TOM core complex was eluted by a linear salt gradient from 0 to 400 mM KCl.

Isolation of Tom40

Addition of 3% *n*-octyl β-D-glucopyranoside (OG) to TOM core complex leads to dissociation of the core complex into the individual components (10). Based on this observation, a protocol was developed to isolate Tom40 protein. Purified mitochondria of the *N. crassa* strain GR-107 were solubilized in 1% DDM, 20% glycerol, 300 mM NaCl, 20 mM imidazole, 20 mM Tris (pH 8.5), and 1 mM PMSF for 30 min at 4°C. After ultracentrifugation at 130,000 $\times$ *g* the clarified extract was bound to a Ni-NTA column (GE Healthcare). The column was rinsed with 0.1% DDM, 10% glycerol, 300 mM NaCl, 20 mM Tris (pH 8.5), then with 10% glycerol, 50 mM K-acetate, 10 mM Mops (pH 7.2, SB-buffer) supplemented with 0.1% DDM. Tom40 was then eluted in SB with 3% OG. Tom22 and other bound proteins were eluted with 300 mM imidazole in SB containing 0.1% DDM. For electrophysiological measurements isolated Tom40 and TOM core complex were further purified via a Superose 6 gel filtration column (GE Healthcare) using SB containing 0.1% DDM.

Electrophysiology

Purified Tom40 as well as TOM core complex protein was reconstituted into black lipid membranes and single channel currents were recorded according to standard protocols (10,45,46). A 1% solution of diphytanoyl phosphatidyl choline (Avanti Polar Lipids, Alabaster, AL) in *n*-decane/butanol (9:1) was painted over a circular hole of 300 μm diameter in the partitioning wall of a custom built Teflon bilayer chamber (47) or in a cylindrical Delrin cup of a bilayer chamber (BCH-13A, Warner Instruments, Hamden, CT). The chamber was filled with symmetrical KCl saline (1 M KCl, 10 mM Hepes, pH 7.0), unless otherwise noted. Protein was added to the *cis*-side of the membrane. Current fluctuations through single channels were recorded using an EPC-8 patch-clamp amplifier (HEKA Electronics, Lambrecht/Pfalz, Germany) in voltage-clamp mode. The headstage of the amplifier was connected to the bilayer chambers by a pair of Ag/AgCl pellet electrodes (WPI, Berlin, Germany). Current signals were low-pass filtered at 3 kHz using the built-in Bessel-filter of the amplifier and monitored for channel insertion using an analog oscilloscope (HAMEG, Mainhausen, Germany). Current and voltage signals from the amplifier were digitized at a sampling rate of 10 kHz per channel using a NI-USB-6251 interface (National Instruments, Munich, Germany) controlled by a program of the Strathclyde electrophysiology suite (WinEDR 2.8 or WinWCP 3.6, J. Dempster, University of Strathclyde, Glasgow, UK). For current-voltage analysis currents were recorded in response to either linear voltage ramps or stepwise voltage changes of 1 or 10 mV increments and 10 s duration per step.

Data analysis and modeling

Digitized current traces were analyzed using software developed in our laboratory in conjunction with standard scientific graphic software (Microcal Origin 7.5, OriginLab, Northhampton, MA).

For the construction of I/V curves and state occupancy plots, stationary current recordings at different voltages of representative experiments were imported into Origin. From these traces all-point histograms were generated and fitted with multiple Gaussian peak functions using nonlinear curve fitting facility in Origin. For each peak, the mean position (current amplitude) and the relative peak area (occupancy probability) were determined at a corresponding holding potential. For each conductance state the results of several experiments were averaged and plotted against the respective holding potential. All values are given as mean $\pm$ SE.

The conductivity for each state was calculated as the slope of the I/V-relation of that state around its reversal potential at 0 mV. The mean open probability p_0 was determined as the relative peak area under current amplitude histograms of the main conductance state S5. For fitting the nonlinear I/V-relations of the low conductance substates we used Nernst-Planck models for ion permeation through a pore with an energy barrier (48). The barrier was considered to follow a symmetrical triangular function with height Φ and width d. By introducing the dimensionless variable $u = z\,q_e V/2k_B T$ the membrane current was then modeled according to:

$$I = \frac{2Azq_eD}{d}\,e^{-\phi}\,(c_1e^{u} - c_2e^{-u})\Big/\left(\frac{e^{(u-\phi)}-1}{u-\phi} + \frac{1-e^{-(u+\phi)}}{u+\phi}\right),$$

where V is the voltage across the membrane and A is the cross-sectional area of the channel (49). The parameters c_1, c_2, D, z, and q_e represent the

concentrations on the left and right boundaries of the channel, the diffusion constant, the valence of the permeant species and the elementary charge. The barrier height and the cross-sectional area of the channel were used as free fitting parameters. k_BT was equal to 4.116×10^{-21} J.

Transitions between different conductance states were made visible by creating mean-variance plots according to Patlak (50,51). A sliding window with a width of 15 data points was moved one step at a time along the current trace. For each step the mean and variance of the data within the window were calculated and plotted versus each other. In this type of plot, transitions between current levels appear as parabolic arches that connect clusters of points with low variance that represent the stable current levels.

For kinetic analysis, stationary single channel records were idealized and analyzed using software developed in our own laboratory. As a first step to idealization, the data were separated into segments using a difference threshold technique (52,53) suitable for recordings with multiple conductance levels. The segments were then classified according to their mean amplitude into conductance levels using a half-amplitude threshold discriminator for multiple levels. Consecutive segments belonging to the same conductance class were merged and the results were stored as a list of ''events'' where each event is a tuple containing (among others) the start time, duration and the mean amplitude of the merged segment along with its conductance class.

Due to the flickering activity of the channels some of the records contained large amounts of very short events where both duration and amplitude were ill defined. These events had to be excluded from the analysis by using a defined dead time (usually one or two sampling intervals). Events shorter than this dead time were marked as invalid but were not removed from the event list or merged into other events. Event list data were then used for kinetic analysis e.g., to construct dwell-time histograms (54,55) for each subconductance state or to estimate various gross kinetic parameters such as mean transition frequencies and mean transition rates between the different conductance states.

To establish a preliminary kinetic scheme for the gating behavior of TOM channels we estimated the gross frequency of transitions from conductance states $i \rightarrow j$, which is a matrix $\boldsymbol{T}$ with entries

$$t_{ij} = \frac{n_{i\rightarrow j}}{n},$$

and the matrix of mean transition rates $\boldsymbol{K}$ with entries

$$k_{ij} = \frac{n_{i\rightarrow j}}{\sum_{n_{i\rightarrow j}} \tau_{i\rightarrow j}},$$

where n is the total number of events, $n_{i\rightarrow j}$ is the number of transitions from conductance state $i \rightarrow j$, and $\tau_{i\rightarrow j}$ is the dwell time (event length) of an event of conductance state i with a transition to state j. The parameters of several recordings ($n = 5$) were combined and imported into Origin and plotted against the applied voltage to determine which rates were voltage sensitive and to estimate their voltage sensitivity.

Kinetic modeling of single channel currents according to the resulting kinetic scheme was done using QuB (56,57).

RESULTS

Isolation of TOM core complex and Tom40

The TOM core complex containing all established components was purified from isolated mitochondria according to established procedures (44). The isolation of Tom40 was based on the dissociation of isolated TOM core complex by the detergent *n*-octyl β-D-glucopyranoside (OG). For this, mitochondria from a *N. crassa* strain containing a hexahistidinyl-tagged form of Tom22 were solubilized in *n*-dodecyl β-D-maltoside and loaded onto a Ni-NTA affinity column. Fig. 1 *A* shows a SDS-polyacrylamide gel of the main fraction after elution of protein with OG and imidazole. The OG fraction contained high yield of virtually pure Tom40 (Fig. 1 *B*). For the electrophysiological measurements isolated Tom40 and TOM core complex were further purified by an additional gel filtration step (data not shown).

Gating behavior and substates of TOM core complex

To gain insights into the biophysical properties of the preprotein translocase of the outer membrane of mitochondria, we have reconstituted TOM core complex from *N. crassa* in planar lipid bilayers and recorded single-channel currents under voltage clamp conditions.

Fig. 2 *A* shows typical single-channel records from membranes clamped to voltages between −100 and +100 mV. Membranes were kept at 0 mV for 10 s and then switched to the test voltage and the currents were recorded. Only current traces during the test pulse are shown. They show a complex gating behavior with transitions between six current levels corresponding to one closed (S0) and five conductive states (S1–S5). The corresponding amplitude histograms are shown in Fig. 2 *B*. To visualize the connectivity between these subconductance states, we subjected all current traces to mean-variance analysis (50,51). The mean-variance plots (Fig. 2 *C*) of the current traces presented in Fig. 2 *A* showed a complex transition pattern that was strongly voltage-dependent and characteristic for TOM channels. This pattern

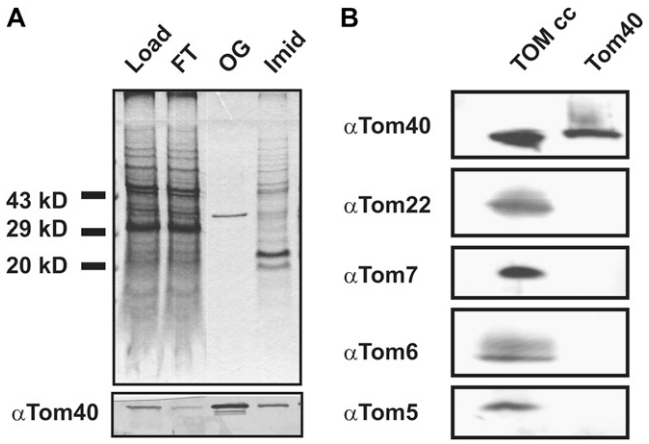

FIGURE 1 Purification of Tom40. (*A*) Mitochondria from a *N. crassa* strain carrying a hexahistidinyl tag on Tom22 were solubilized in 0.3% DDM and passed through a Ni-NTA affinity column. After various washing steps Tom40 was eluted with 3% OG; Tom22 among other proteins was eluted with 300 mM imidazole. Aliquots of the resulting column fractions were analyzed by Coomassie blue stained tricine gels and with Western blots. (*Lane 1*) Mitochondria; (*lane 2*) flow through; (*lane 3*) OG eluate; (*lane 4*) imidazole eluate. (*B*) The purity of isolated Tom40 was assessed by Western blot analysis using antibodies against Tom40, Tom22, Tom7, Tom6, and Tom5.

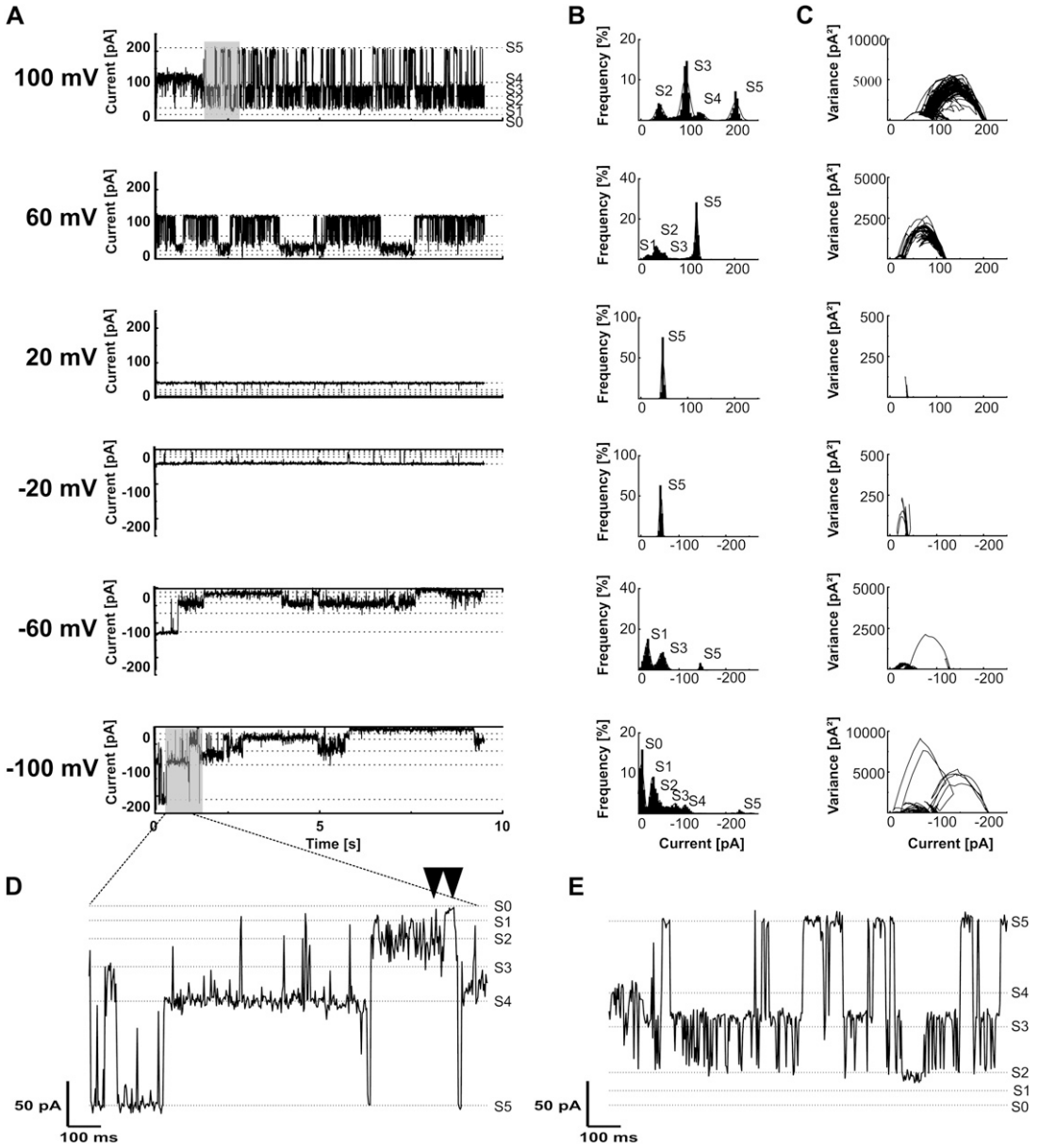

FIGURE 2 Current fluctuations through single TOM core complex channels. (*A*) Purified TOM core complex was reconstituted into planar lipid bilayers and membrane currents were recorded in symmetrical 1 M KCl, 10 mM Hepes, pH 7.0 using the voltage clamp technique with clamp potentials between −100 and +100 mV. At low voltages between −20 and +20 mV hardly any voltage-dependent gating was observed. At higher voltages, TOM-mediated currents were voltage-sensitive and switched between six nonequidistant conductance states (S0–S5). The conductance states S0–S5 are indicated as dotted lines. (*B*) Amplitude histograms (bin widths, 4 pA) produced from 10 s of channel activity. Up to six peaks are evident in the histograms (*lower panel*) and are labeled with the corresponding subconductance level. Gaussian curves were fitted to the data and are superimposed to the histograms. (*C*) Mean-variance plots of the recordings shown in (*A*). The window widths used were 15 points, corresponding to 1.5 ms. Transitions between conductance states are visible as parabolic arches in the plots connecting low variance current levels. (*D* and *E*) Enlarged view of the shaded areas shown in (*A*). (*D*) Currents at −100 mV. (*E*) Currents at +100 mV. Arrows indicate sojourns in the closed state S0.

was distinctively different to currents from VDAC, the predominant channel protein of the mitochondrial outer membrane (data not shown).

At high positive potentials (>60 mV), the channels flickered rapidly between conductance states S5, S3, and S2 with very brief sojourns in S5. At lower positive voltages the sojourns in the open state S5 became more frequent and the overall occupancies of the higher conductive states increased. ''Bursts'' of transitions between S5 and S3 were interspersed with periods where the channel predominantly occupied states S4 and S2. Transitions to the states S1 and S0 occurred less frequent (Fig. 2 *D*) and became visible only in longer recordings ($t > 60$ s). At zero voltage, the occupancy of the S5 state was close to unity. At negative potentials the occu-

pancies of the higher conductive states again decreased, however, the sojourns in S5 and particularly in S2 were longer with less flickering between states.

The very fast flickering at positive potentials (Fig. 2 *E*) is typical for this polarity and can be used to distinguish the direction of insertion the channel in different recordings. In all subsequent figures, the voltage polarities of the records were, therefore, aligned accordingly.

I/V characteristics and selectivity of TOM core complex channels

To characterize the conductivity of sublevels S1 to S5 we have used linear and stepped voltage ramps to generate current-voltage (I/V) curves (Fig. 3 *A*). As shown in Fig. 3 *A* and Fig. 3 *B*, the conductance states S5 and S4 followed a linear current-voltage relation within the tested voltage range of ± 120 mV. From n = 93 records we have determined the conductivity in 1 M KCl for S5 and S4 as 2.16 ± 0.34 nS and 1.09 ± 0.15 nS, respectively. The conductance states S3, S2, and S1, on the other hand, did not show a linear characteristic but followed a current-voltage relation with increasing conductivity at high voltages. In the linear voltage range at $|V| <$ 50 mV states S3, S2, and S1 we have estimated a conductivity of 0.67 ± 0.09 nS, 0.36 ± 0.06 nS, and 0.16 ± 0.03 nS, respectively.

Recordings of I/V curves in asymmetric salt solutions eventually allowed the determination of the ratio of the cation to anion permeability of the TOM core complex channel (data not shown). A ratio of ~1.7 was in agreement with previous reports (8) and indicated that the channel is slightly cation selective.

Concentration dependence of the conductivity

To facilitate comparison between previously published data from our laboratory and others, we have also measured the dependence of the conductivity on the salt concentration. Similar patterns of conductance levels were observed in the presence of 125, 250, and 1000 mM KCl (Fig. 3, *D–F*). The conductivity of all states followed a Michaelis-Menten relation of the form $\gamma = \gamma_{max} c/[K_s + c]$ (36). The unit conductance (S5-state) of TOM core complex channels measured at 125 mM and 250 mM KCl was 0.41 ± 0.09 nS ($n = 4$) and

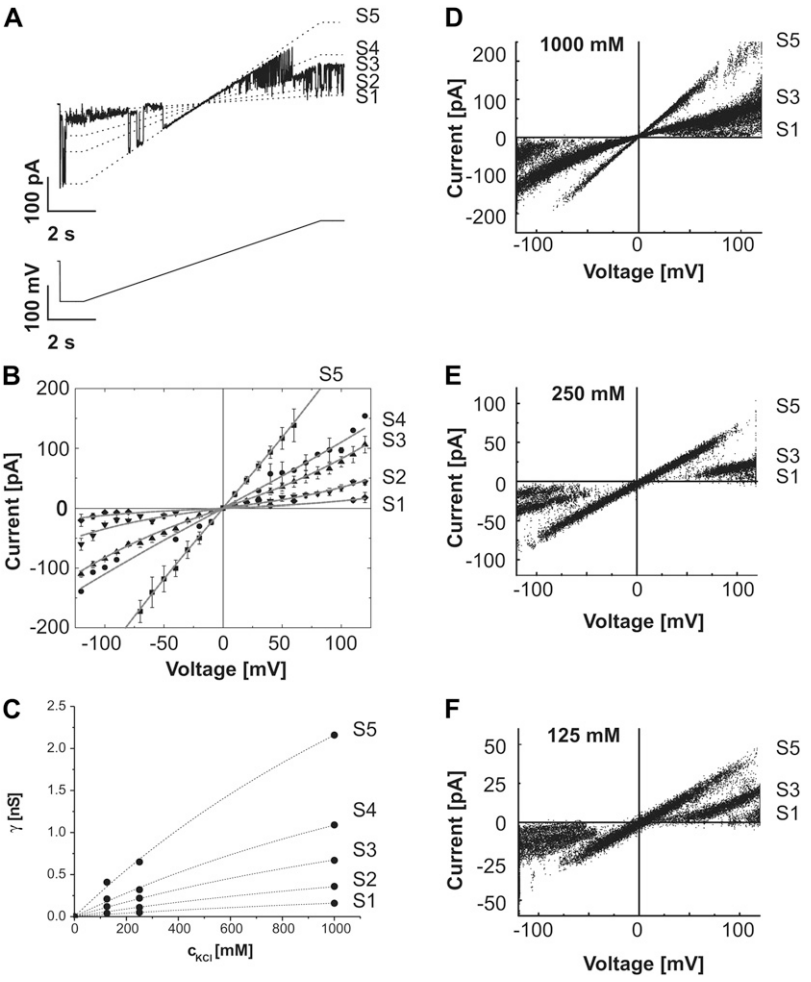

FIGURE 3 I/V characteristic of TOM channel conductance states. (*A*) A representative current trace of a single TOM core complex channel recorded in 1 M KCl, 10 mM Hepes, pH 7.0 (*upper panel*), in response to a linear voltage ramp from −120 to +120 mV (*lower panel*). The conductance states S1 to S5 are indicated as dotted lines. (*B*) I/V characteristic from mean current amplitudes determined by fits to current histograms for substates S1 to S5. Deviation from linear (ohmic) I/V relation with a typical inverted *S*-shape is particularly evident for the S3 state but also with S2 and S1. The data were fitted with a Nernst-Planck permeation model assuming a single energy barrier in the middle of the pore (*solid lines*). All fits were based on a channel length of 70 Å (44) an ion diffusion constant of 2×10^{-9} $m^2 s^{-1}$ (36) and a symmetrical salt concentration of 1 M KCl at both boundaries of the channel. (*C*) Concentration dependence of the conductivities as determined in (*D–F*). Conductivities follow a Michaelis-Menten relation with an apparent K_S of 2.6 ± 0.8 M and a maximum conductivity γ_{max} of 7.7 ± 1.7 nS for the main open state S5. (*D–F*) I/V curves of single TOM core complex channels were recorded in 125 mM, 250 mM, or 1 M KCl, 10 mM Hepes, pH 7.0, as described in (*A*). Data of 20 voltage ramps were superimposed. The I/V curves for substate S5 are virtually linear in all three salt solutions. I/V relationships of the lower conductance states S3 and S2 display a nonlinear behavior with increasing conductance at high potentials.

0.65 ± 0.05 nS ($n = 4$), respectively (Fig. 3 *C*). This corresponds to an apparent K_S of 2.6 ± 0.8 M and a maximum conductivity γ_{max} of 7.7 ± 1.7 nS. The conductivities of all subconductance states are summarized in Table 1.

Voltage-dependent substate occupancies of TOM core complex channels

Next, we investigated the voltage-dependence of TOM core complex channels. We have determined the occupancy probability of all substates S1 to S5 at different transmembrane potentials (Fig. 4). Current traces were recorded at constant voltage and the occupancy probabilities were calculated as relative peak areas from Gaussian fits to the corresponding amplitude histograms.

At low potentials ($|V| < 20$ mV) the TOM channel resided predominantly in its main conductive state S5. At intermediate voltages (20 mV $< |V| <$ 100 mV), the complex switched to states S4, S3, and S2, whereas S4 had a significantly smaller occupancy probability than S3 and S2. S1 was occupied at high voltages of $|V| > 100$ mV, only. The closed state S0 was only rarely observed. The occupancy probability of state S5 followed an asymmetric bell shaped curve and could be fitted by a double Boltzmann equation of the form

$$p = 1/\left(\left(1 + e^{-A(V-V_o)}\right)\left(1 + e^{-A'(V-V_0')}\right)\right),$$

where V_0 and V_0' are the voltages at which the open probability p is half maximal, and A and A' are the voltage sensitivities of the occupancy probability. The curve parameters are $V_0 = -33 \pm 7$ mV, $V_0' = 68 \pm 10$ mV, $A = 0.1 \pm 0.03$ mV^{-1} and $A' = -0.06 \pm 0.02$ mV^{-1} corresponding to an equivalent gating charge $z\delta = 2.5 \pm 0.8$ and $z\delta' = 1.5 \pm 0.5$, respectively.

Voltage-dependent gating kinetics of TOM core complex channels

We have further investigated the kinetics of the channel by estimating the mean transition rates between conductance states $k_{ij} = 1/\overline{\tau_{ij}}$ from the mean dwell times τ_{ij} of events in state *i* that were followed by a transition to state *j*. These data were calculated directly from event lists rather than from dwell-time histograms because due to the limited record length, for some transitions, the number of available events was not sufficient to create meaningful histograms.

The resulting rate estimates were then plotted versus the applied transmembrane potential and fitted with $k_{ij}(V) = k_{ij}^* e^{\lambda_{ij} V}$, where k^* is the rate at 0 mV and λ is the voltage sensitivity of the rate. An example of this analysis is shown in Fig. 5 *A* for the rates for transitions S5 → S3. As the rate data cover more than two orders of magnitude, they were plotted in logarithmic scale. Exponential voltage dependence, therefore, shows as a linear correlation of data points in the plots. The rates showed bimodal voltage dependence with a symmetry about 0 mV. Therefore, each polarity of the transmembrane potential was fitted separately, which is equivalent to saying that the data are a superposition of two transitions between e.g., S5 → S3 for positive potentials and S5 → S3′ for negative potentials (The complete matrix of plots for all transitions are given in Supplementary Materials, Fig. S1. Bimodal voltage dependence was present for almost all subconductance-state transitions observed. In the case shown, both rates were voltage-dependent and almost mirror images about a symmetry axis at 0 mV. However, for some of the rates we found that they were voltage-independent for either one or both polarities. In addition to the rates we have also determined the relative frequency of occurrence of transitions within a record. These plots were then used to draft the kinetic scheme of the TOM core complex channel (Fig. 5 *B*). Transitions with consistently low frequency of occurrence (<5%) over the whole voltage range were excluded. Fig. 5 *B* shows the simplest kinetic model that was consistent with the steady-state occupancies in Fig. 4. The model consists of 10 kinetic states and 16 transitions. The parameters are summarized in Table 2.

The data shown were collected from five independent bilayer experiments. In total $n = 102$ records were analyzed covering a voltage range of ±120 mV; the time resolution of the records was ~1 kHz, therefore, the fastest rate visible in our analysis is ~500 s^{-1}.

Gating behavior of TOM core complex channels lacking Tom5, Tom6, or Tom7

To test how the small Tom proteins Tom7, Tom6, and Tom5 affect the conductivity pattern and the gating kinetics of the TOM complex we compared the channel activity of wild-type TOM core complex and TOM core complex lacking

TABLE 1 Concentration dependence of substate conductivities of TOM core complex channels

	125 mM	250 mM	1000 mM	γ_{max}	K_S
γ_{S1}	n.d.	0.05 ± 0.01 nS	0.16 ± 0.03 nS	n.d. nS	n.d.
γ_{S2}	0.04 ± 0.01 nS	0.11 ± 0.02 nS	0.36 ± 0.06 nS	3 ± 30 nS	4.2 ± 6 mol/l
γ_{S3}	0.12 ± 0.01 nS	0.22 ± 0.02 nS	0.67 ± 0.09 nS	3 ± 10 nS	2.2 ± 8 mol/l
γ_{S4}	0.21 ± 0.02 nS	0.32 ± 0.01 nS	1.09 ± 0.15 nS	7 ± 23 nS	3.6 ± 12 mol/l
γ_{S5}	0.41 ± 0.09 nS	0.65 ± 0.05 nS	2.16 ± 0.34 nS	13 ± 19 nS	3.2 ± 5 mol/l

The conductivities shown are from the chord conductance of the I/V characteristics around 0 mV transmembrane potential. Due to the nonlinearity of the I/V relations of S1–S3 these are lower limits. n.d., not determined.

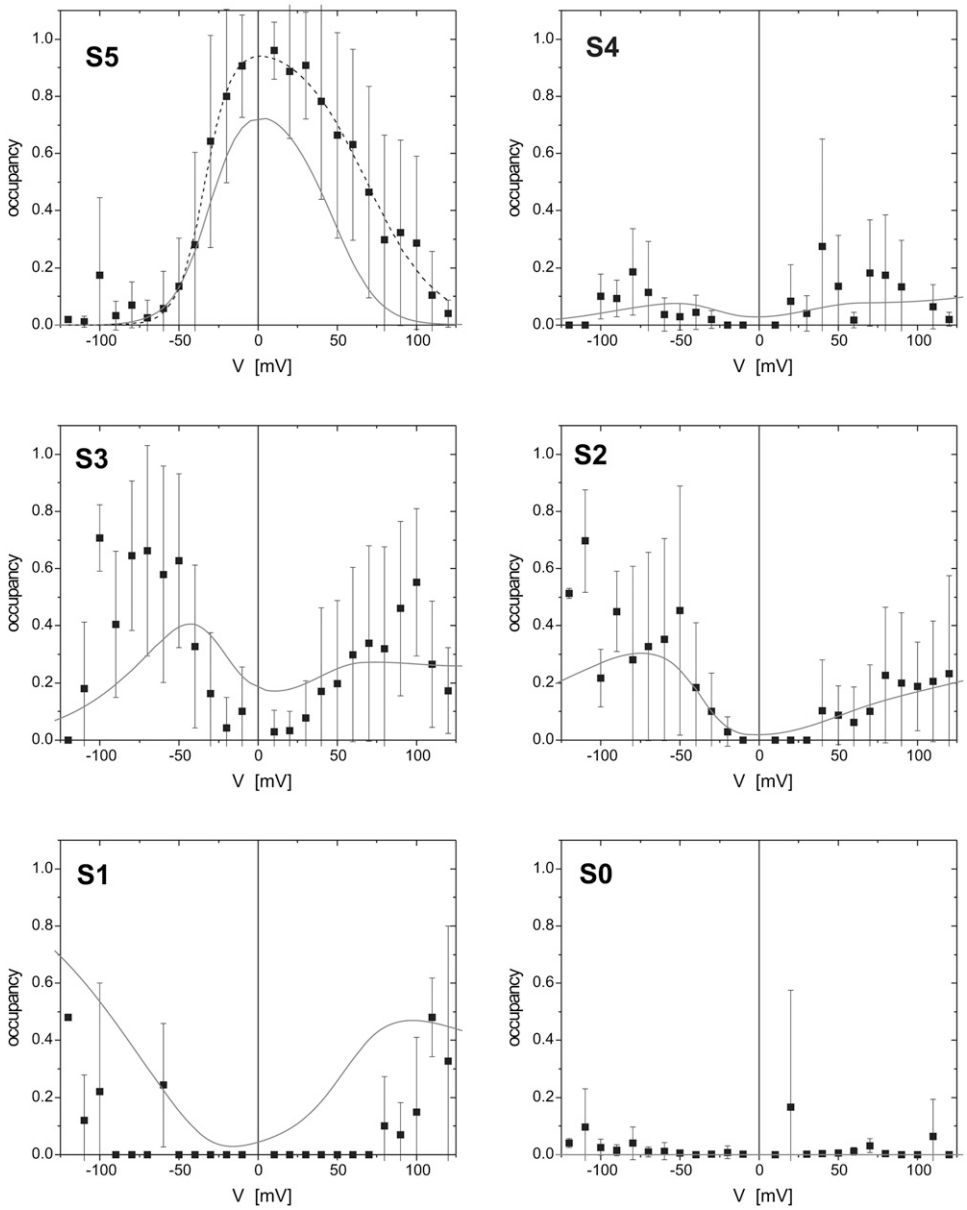

FIGURE 4 Voltage-dependent state occupancies of TOM core complex channels. Voltages from −120 to +120 mV were applied in increments of 10 mV to single TOM core complex channels. Membrane currents were measured for 10 s each ($n = 8$). For each voltage all-point histograms were generated and fitted with Gaussian functions. The occupancy probabilities p of the substates S0–S5 were obtained from the area below each peak at the indicated potentials. The probability of state S5 was fitted to a double Boltzmann distribution (*dotted line*) with parameters $V_0 = -33 \pm 7$ mV, $V_0' = 68 \pm 10$ mV, $A = 0.1 \pm 0.03$ mV^{-1} and $A' = -0.06 \pm 0.02$ mV^{-1}, respectively. The solid lines represent the subconductance state occupancy probabilities predicted by the kinetic model in (Fig. 5 *B*).

Tom5, Tom6, or Tom7. This was purified from detergent solubilized mitochondrial outer membrane vesicles of *N. crassa* strains *tom5RIP*, *tom6RIP*, and *tom7KO-35* (13,18) by using anion exchange and gel filtration chromatography. Electrophysiological analysis of TOM core complex deficient in Tom5, Tom6, or Tom7 showed similar channel activity as wild-type complex (Fig. S2).

Gating behavior of purified Tom40 channels

Previous studies have shown that Tom40 is the main component of the TOM complex that forms the conductive pore of the outer mitochondrial membrane (9–11) whereas Tom22 has been suggested to play a role in regulating the open probability of the channel (16).

Purified Tom40 reconstituted into planar lipid bilayers formed cation selective channels similar to TOM core complex (data not shown). Analysis of $n = 119$ insertion events of Tom40 into lipid bilayers exhibited four conductivities (S2*–S5*) that corresponded roughly to states S2, S3, S4, and S5 of the core complex (Fig. 6, *A* and *B*). The conductivities in 1 M KCl were 0.42 ± 0.03 nS, 0.81 ± 0.03 nS, 1.41 ± 0.02 nS, and 2.01 ± 0.02 nS. Tom40 channels with a conductance corresponding to the S1 state of the core complex have not been observed.

Application of linear voltage ramps from −70 to +70 mV resulted in linear current responses with very little gating transitions (Fig. 6 *C*). Increasing the voltage range to ±150 mV, however, led to voltage-dependent closures (Fig. 7) similar to those of TOM core complex (Fig. 7 *B*). The

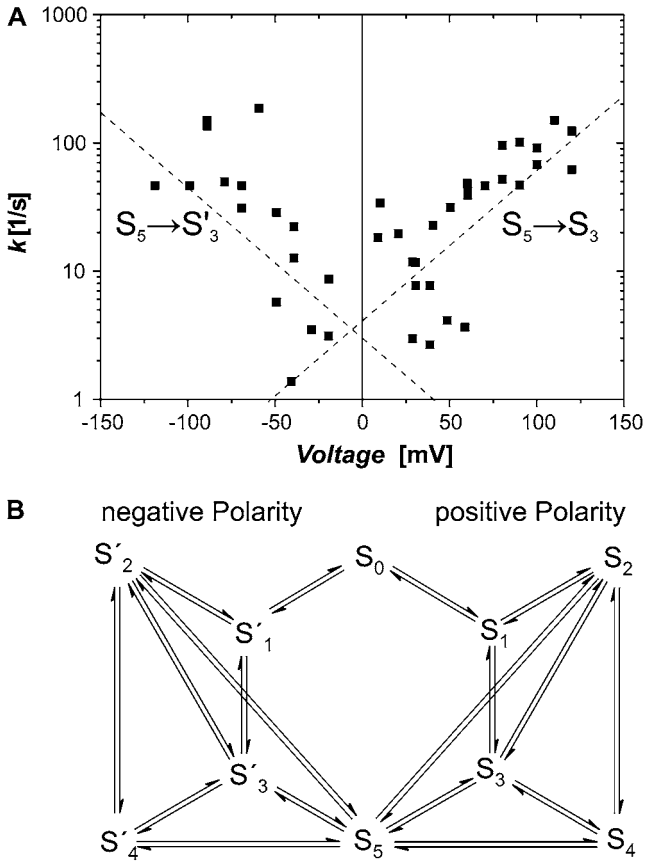

FIGURE 5 Voltage-dependent rates of TOM core complex channels. (*A*) Voltage dependence of the transition rate between conductance states S5 → S3. Due to the logarithmic scaling of the ordinate, voltage-dependent rates are represented as linearly correlated clusters of data points. Note the bimodal V-shaped relation that indicates that transitions from conductance states S5 to S3 are governed by two almost symmetric processes with rates $k_{S_5\rightarrow S_3}$ and $k_{S_5\rightarrow S'_3}$. In this particular case both rates were voltage-dependent with $k^*_{S_5\rightarrow S_3} = 21 \pm 9\ s^{-1}$ and $\lambda_{S_5\rightarrow S_3} = 0.013 \pm 0.005\ V^{-1}$ and $k^*_{S_5\rightarrow S'_3} = 9 \pm 10\ s^{-1}$ and $\lambda_{S_5\rightarrow S'_3} = -0.017 \pm 0.012\ V^{-1}$. (*B*) Topology for the kinetic scheme for TOM core complex gating. The S_X-notation of the kinetic states refers to the conductance class whereas the $S \leftrightarrow S'$ notation indicates the different polarity of the voltage dependence.

threshold voltage for closing the channel decreased for each consecutive voltage ramp. This effect was reversible when returning to ramps with a small voltage range.

DISCUSSION

In the presence of preprotein peptides, TOM channels have been observed to show a typical flickering block (10,26, 30,58). This blockage is also voltage sensitive, roughly following a Woodhull formalism (20,59). This suggests a mechanism for protein translocation through TOM by threading the polypeptide chain through the open pore of the TOM channel. If this assumption holds, then more detailed information about the threading mechanism could be obtained from analysis of amplitude and duration of the blockage events similar to reports on polynucleotide and peptide translocation through pores formed by *Staphylococcus aureus* α-hemolysin (37,38,40,41,60–62). This, however, is hampered by the endogenous behavior of the channel that often resembles the behavior that would be expected for open channel blockage by a charged blocking particle.

In our hands, reconstituted TOM core complex channels show a very rich behavior that appears much more complex than might be anticipated from previous reports (8–11, 30,44). We have, therefore, started to characterize the voltage-dependent behavior of the channels without blocking peptides to compare the endogenous behavior to that induced by mitochondrial presequence peptides.

Conductance levels

In this report, we have identified at least six electrically distinct conductance states of the TOM core complex channel (S0–S5). The transitions among these are coupled to the membrane voltage and are modulated by the presence of the small Tom subunits (Tom22, Tom7, Tom6, and Tom5) but not by Tom7, Tom6, and Tom5 alone. The predominant conductance states of the channel are the main open state S5 and the two intermediate states S3 and S2.

Although multiple open conductance states in the TOM core complex have been reported previously (9,20,26,34) no detailed characterization has been available so far. Previous studies on mitochondrial outer membranes and TOM complex channels of *S. cerevisiae* and *N. crassa* have focused on transitions between three approximately equidistant conductance levels (8,9,11,26,30,34) suggesting a ''double-barrel'' model similar to that proposed for the ClC-0 chloride channel (63,64). In our records we did not observe equal spacing of the conductance levels and the transitions between them (see Table 2, *last column*), except at high voltages, where states S1, S2, and S3 display nonlinear I/V characteristics. This data, therefore, clearly argues against such a simple view. Because the occupancy probabilities of all subconductance states depend on membrane potential, not all subconductances are visible at a given voltage. Thus, earlier studies may have overlooked the open conductance levels S1, S2, and S4. In patch clamp recordings, the presence of the S1 state may have been mistaken for a finite seal conductance and therefore assigned to a fully closed state. In our recordings the nonconductive state S0 can be distinguished clearly from S1. It has the conductivity of a protein-free lipid bilayer ($R >$ 30 GΩ in 1 M KCl).

I/V relation

For the main conductance state S5 and subconductance S4 TOM core complex channels exhibited a linear (ohmic) I/V relationship consistent with a straight cylindrical pore model (36). By contrast, the lower subconductance states S1 to S3 followed inverted *S*-shaped I/V curves where the current

TABLE 2 Rates and voltage sensitivities of TOM core complex channels

Transition	k^* [s^{-1}]	λ [V^{-1}]	Transition	k^* [s^{-1}]	λ [V^{-1}]	$\Delta\gamma$ [nS]
$S_0 \rightarrow S_1$	3000 ± 400	−0.053 ± 0.002	$S_1 \rightarrow S_0$	170 ± 25	−0.017 ± 0.001	0.2
$S_0 \rightarrow S'_1$	7500 ± 700	0.09 ± 0.002	$S'_1 \rightarrow S_0$	350 ± 80	−0.046 ± 0.004	0.2
$S_1 \rightarrow S_2$	270 ± 200	−0.019 ± 0.009	$S_2 \rightarrow S_1$	20 ± 15	0.02	0.2
$S_1 \rightarrow S_3$	120 ± 13	—	$S_3 \rightarrow S_1$	130 ± 30	—	0.5
$S_2 \rightarrow S_3$	50 ± 60	0.006 ± 0.010	$S_3 \rightarrow S_2$	110 ± 12	—	0.3
$S_2 \rightarrow S_5$	200 ± 70	−0.004 ± 0.006	$S_5 \rightarrow S_2$	1.5 ± 1.5	0.03 ± 0.01	1.8
$S_3 \rightarrow S_4$	102 ± 15	—	$S_4 \rightarrow S_3$	480 ± 350	−0.021 ± 0.009	0.4
$S_3 \rightarrow S_5$	200 ± 67	−0.008 ± 0.005	$S_5 \rightarrow S_3$	21 ± 9	0.012 ± 0.005	1.5
$S_4 \rightarrow S_5$	170 ± 18	—	$S_5 \rightarrow S_4$	8 ± 7	0.021 ± 0.009	1.1
$S_5 \rightarrow S'_2$	2.4 ± 1.2	−0.023 ± 0.005	$S'_2 \rightarrow S_5$	700 ± 800	0.05 ± 0.03	1.8
$S_5 \rightarrow S'_3$	9 ± 10	−0.02 ± 0.01	$S'_3 \rightarrow S_5$	56 ± 17	—	1.5
$S_5 \rightarrow S'_4$	3 ± 2	−0.027 ± 0.007	$S'_4 \rightarrow S_5$	170 ± 18	—	1.1
$S'_1 \rightarrow S'_2$	90 ± 100	0.01 ± 0.02	$S'_2 \rightarrow S'_1$	80 ± 20	—	0.3
$S'_1 \rightarrow S'_3$	300 ± 150	0.03 ± 0.01	$S'_3 \rightarrow S'_1$	1.3 ± 0.7	−0.034 ± 0.005	0.2
$S'_2 \rightarrow S'_3$	15 ± 10	−0.010 ± 0.008	$S'_3 \rightarrow S'_2$	3 ± 5	−0.02 ± 0.016	0.3
$S'_3 \rightarrow S'_4$	54 ± 8	—	$S'_4 \rightarrow S'_3$	600 ± 400	0.03 ± 0.01	0.4

Transitions where no voltage sensitivities λ are shown are voltage independent.

increased faster than the voltage. This observation indicates that the TOM channel can switch to a conformation in which the permeating ions sense a repelling force originating either from surface charges or image forces in the pore.

More quantitative information on this interaction can be obtained from fitting the I/V data with a Nernst-Planck barrier model (48,49). Assuming a symmetrical triangular barrier with a fixed width of ~70 Å (pore length as determined by (44)), the I/V curves for states S1–S3 predict an energy barrier of ~3.6, ~2.0, and ~0.7 k_BT. Values of this magnitude are consistent with electrostatic barriers in other ion channels such as the nicotinic acetylcholine receptor or glycine receptor channels (nAChR: ~3 k_BT, GlyR: ~4 k_BT (65)). The energy barrier for substates S4 and S5 was found to be lower (~0.4 k_BT) than those for states S1–S3 consistent with an ohmic channel (36). Because the TOM channels accommodate both cations and anions (8,9,23,58) we would predict that dielectric image forces significantly contribute to this energy barrier.

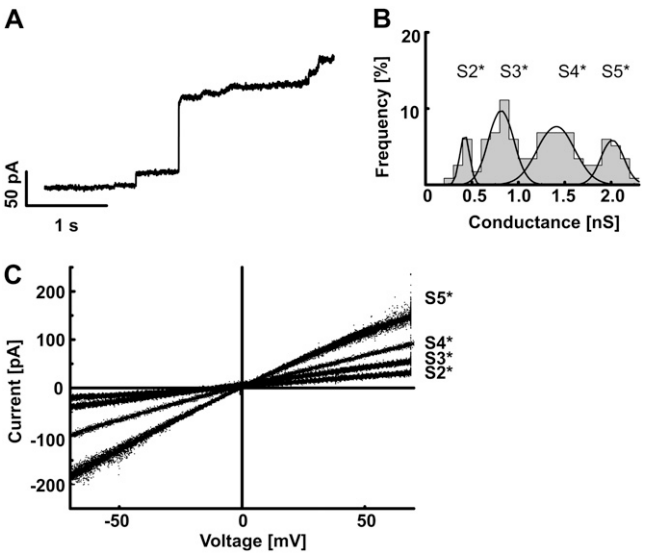

FIGURE 6 Properties of single channels of Tom40. (*A*) Purified Tom40 was added to one side of a planar lipid membrane and single channel currents were measured in the presence of a membrane potential of 70 mV. *S*tep-like increases in current levels indicate incorporation of Tom40 channels into the bilayer. The aqueous phase contained 1 M KCl, 10 mM Hepes, pH 7.0. (*B*) Histogram of channel conductances. A total of $n = 119$ conductance increments as shown in (*A*) was analyzed. *S**, conductance states of Tom40. (*C*) I/V curves of single Tom40 channels recorded by application of linear voltage ramps between −70 and +70 mV. Four independent recordings with different conductivities were overlaid.

In addition to the barrier height it was also possible to estimate the effective radius of the TOM core complex channel in states S1–S5 ($r_{S1} \approx 5$ Å, $r_{S2} \approx 5$ Å, $r_{S3} \approx 6$ Å, $r_{S4} \approx 7$ Å, and $r_{S5} \approx 9$ Å). These values are consistent with the pore radius determined by electron microscopy ($r \approx 10$ Å (44)). Considering the dimension of an unfolded polypeptide chain the large conductance states S4 and S5 are the likely candidates that represent the protein-conductive pore conformation. Electrophysiological experiments studying the interaction of TOM core complex with model peptides are currently under way.

Voltage dependence

As shown in previous reports, TOM core complex channels show voltage-dependent gating with channel closure on a bell-shaped open probability (66). The main conductance state S5 showed a strong asymmetry of the voltage-dependent open probability and characteristic flickering behavior at one polarity (Fig. 2, *A*, *upper traces*, and *E*). This allowed us to identify the orientation of the channel in the bilayer and align the voltage polarity for the analysis accordingly. Fig. 4 shows the voltage-dependent occupancies of all subconductance levels that were identified in the records of Fig. 2. Note the low occupancy probability of the S4 subconductance level is inconsistent with a binomial distribution of multiple open pores or a kinetic scheme with a sequential arrangement of

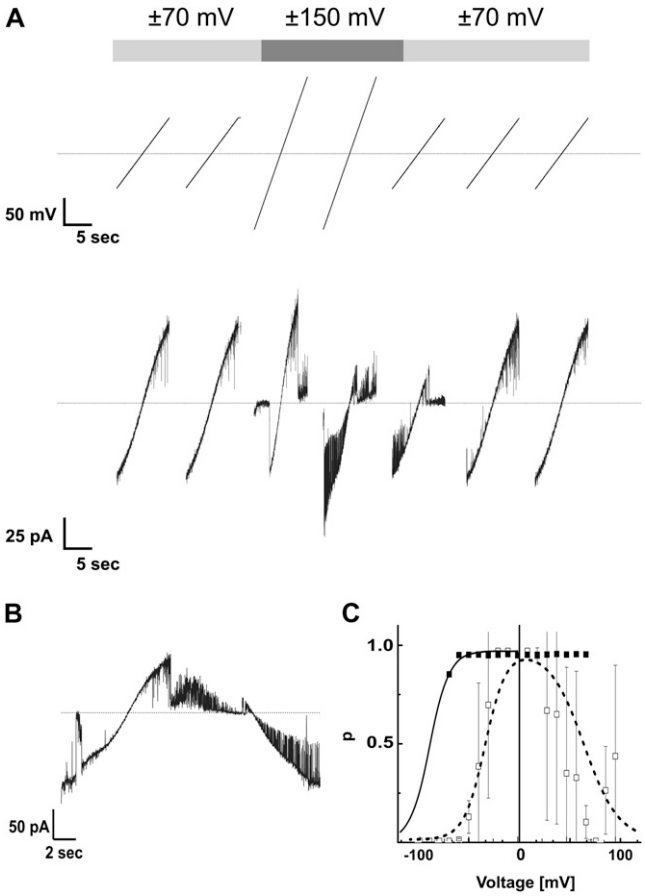

FIGURE 7 Voltage-dependence of single-channels of Tom40. (*A*) Response of a single Tom40 channel to linear voltage ramps of different amplitude ranging from −70 to +70 mV and from −150 to +150 mV. Initially very little gating between substates could be observed; increasing the amplitude of the ramps induced voltage-dependent gating. Subsequent decrease of the voltage amplitude reversed the gating behavior to the initial gating pattern. (*B*) Expanded view of the response of a linear voltage ramp ranging from −150 to +150 mV as in (*A*). (*C*) Open probability of the main conductance state of Tom40 determined as described in Fig. 4. Application of linear voltage ramps from −70 to +70 mV resulted in very few gating transitions (*solid squares*). Increasing the voltage range to ±150 mV led to voltage-dependent closures (*open squares*) approaching the characteristics of TOM core complex (*dashed line*, Fig. 4). For all records, the *cis* and *trans* compartments contained 1 M KCl, 10 mM Hepes, pH 7.0.

the subconductance levels. The kinetic scheme shown in Fig. 5 *B* represents the simplest kinetic model that was qualitatively consistent with the steady-state occupancies and the overall behavior of the channels (Fig. 4, *solid lines*). The deviations from the model predictions, particularly the large main state occupancy around 0 mV may be explained by the relatively short periods used for estimating the occupancies as some of the rate constants span at least three orders of magnitude. Another factor may be the limited time resolution of the data, which cuts off the visible rate constants at ~500 s^{-1} and, therefore, probably leads to an underestimation of both rates k^* and voltage sensitivities λ of the fast voltage sensitive rates. Both limitations arise from the large orifice (diameter ~300 μm) of the bilayer chamber that was used in these experiments. This produces large bilayer membranes with high capacitance and low stability, particularly at transmembrane potentials above 100 mV. The same limitations also prevented a more rigorous analysis using dwell-time histograms or conditional dwell-time histograms. We were, therefore, unable to distinguish any aggregated kinetic substates within a given subconductance state other than those that were apparent from their different voltage sensitivities (i.e., S_x versus S'_x). In this respect, the model should be regarded as preliminary and represents our current working hypothesis until more detailed data with higher resolution are available.

Tom40 channels

Another interesting finding was that purified Tom40 channels lacking Tom22, Tom7, Tom6, and Tom5 appeared to be ''frozen'' in one of five conductance states. This behavior resembles that of trypsin treated PSC-channels (59,66). However, in our experiments after applying high membrane potentials ($|V| > |100$ mV$|$) transitions between different conductance states similar to normal TOM core complex behavior could be induced. This was reversed after switching back to lower voltages. Because the channel properties of TOM core complex lacking Tom5, Tom6, or Tom7 were similar to those of wild-type core complex, loss of Tom22 is the most likely cause for this effect.

From Fig. 7 *C* we would estimate V_0 for Tom40 to be initially at about −90 mV. Assuming the same voltage sensitivity as in TOM core complex this would correspond to a transition energy of ~9 k_BT that is reduced to 3.3 k_BT after application of higher voltages. Therefore, Tom22 acts as a modulator of the voltage-dependent gating by reducing the initial transition energy by ~6 k_BT.

SUMMARY

In summary, we have shown that the TOM machinery is a highly dynamic structure that can switch between a complex set of functionally distinct conformational states. We have also shown that the low molecular mass Tom subunits (Tom22 and/or Tom5, Tom6, and Tom7) contribute additional flexibility to the TOM complex by significantly reducing the energy required for transitions between some of these states. Future studies using model substrates will have to show the significance of this dynamic behavior for the mechanism of protein translocation.

SUPPLEMENTARY MATERIAL

To view all of the supplemental files associated with this article, visit www.biophysj.org.

The authors wish to thank Beate Rehkopf and Margarida Dias Rodrigues for expert technical help and Dr. Frank Nargang for providing the *N. crassa* mutants tom5RIP, tom6RIP, and tom7KO-35.

This work was supported by the Deutsche Forschungsgemeinschaft (Nu75/2) and the Volkswagen Foundation to S.N.

REFERENCES

1. Braun, H. P., and U. K. Schmitz. 1999. The protein-import apparatus of plant mitochondria. *Planta*. 209:267–274.
2. Lithgow, T. 2000. Targeting of proteins to mitochondria. *FEBS Lett.* 476:22–26.
3. Pfanner, N., and A. Geissler. 2001. Versatility of the mitochondrial protein import machinery. *Nat. Rev. Mol. Cell Biol.* 2:339–349.
4. Pfanner, N., N. Wiedemann, C. Meisinger, and T. Lithgow. 2004. Assembling the mitochondrial outer membrane. *Nat. Struct. Mol. Biol.* 11:1044–1048.
5. Rehling, P., K. Brandner, and N. Pfanner. 2004. Mitochondrial import and the twin-pore translocase. *Nat. Rev. Mol. Cell Biol.* 5:519–530.
6. Neupert, W. and J. M. Herrmann. 2007. Translocation of proteins into mitochondria. *Annu. Rev. Biochem.* 76:6.1–6.27.
7. Prokisch, H., S. Nussberger, and B. Westermann. 2002. Protein import into mitochondria of Neurospora crassa. *Fungal Genet. Biol.* 36:85–90.
8. Künkele, K. P., S. Heins, M. Dembowski, F. E. Nargang, R. Benz, M. Thieffry, J. Walz, R. Lill, S. Nussberger, and W. Neupert. 1998. The preprotein translocation channel of the outer membrane of mitochondria. *Cell*. 93:1009–1019.
9. Hill, K., K. Model, M. T. Ryan, K. Dietmeier, F. Martin, R. Wagner, and N. Pfanner. 1998. Tom40 forms the hydrophilic channel of the mitochondrial import pore for preproteins. *Nature*. 395:516–521.
10. Ahting, U., M. Thieffry, H. Engelhardt, R. Hegerl, W. Neupert, and S. Nussberger. 2001. Tom40, the pore-forming component of the protein-conducting TOM channel in the outer membrane of mitochondria. *J. Cell Biol.* 153:1151–1160.
11. Becker, L., M. Bannwarth, C. Meisinger, K. Hill, K. Model, T. Krimmer, R. Casadio, K. N. Truscott, G. E. Schulz, N. Pfanner, and R. Wagner. 2005. Preprotein translocase of the outer mitochondrial membrane: reconstituted Tom40 forms a characteristic TOM pore. *J. Mol. Biol.* 353:1011–1020.
12. Dietmeier, K., A. Hönlinger, U. Bömer, P. J. T. Dekker, C. Eckerskorn, F. Lottspeich, M. Kübrich, and N. Pfanner. 1997. Tom5 functionally links mitochondrial preprotein receptors to the general import pore. *Nature*. 388:195–200.
13. Schmitt, S., U. Ahting, L. Eichacker, B. Granvogl, N. E. Go, F. E. Nargang, W. Neupert, and S. Nussberger. 2005. Role of Tom5 in maintaining the structural stability of the TOM complex of mitochondria. *J. Biol. Chem.* 280:14499–14506.
14. Alconada, A., M. Kubrich, M. Moczko, A. Honlinger, and N. Pfanner. 1995. The mitochondrial receptor complex: the small subunit Mom8b/Isp6 supports association of receptors with the general insertion pore and transfer of preproteins. *Mol. Cell. Biol.* 15:6196–6205.
15. Hönlinger, A., U. Bömer, A. Alconada, C. Eckerskorn, F. Lottspeich, K. Dietmeier, and N. Pfanner. 1996. Tom7 modulates the dynamics of the mitochondrial outer membrane translocase and plays a pathway-related role in protein import. *EMBO J.* 15:2125–2137.
16. van Wilpe, S., M. T. Ryan, K. Hill, A. C. Maarse, C. Meisinger, J. Brix, P. J. Dekker, M. Moczko, R. Wagner, M. Meijer, B. Guiard, A. Honlinger, and N. Pfanner. 1999. Tom22 is a multifunctional organizer of the mitochondrial preprotein translocase. *Nature*. 401:485–489.
17. Model, K., C. Meisinger, T. Prinz, N. Wiedemann, K. Truscott, N. Pfanner, and M. Ryan. 2001. Multistep assembly of the protein import channel of the mitochondrial outer membrane. *Nat. Struct. Biol.* 8:361–370.
18. Sherman, E. L., N. E. Go, and F. E. Nargang. 2005. Functions of the small proteins in the TOM complex of *Neurospora crassa*. *Mol. Biol. Cell.* 16:4172–4182.
19. Suzuki, H., T. Kadowaki, M. Maeda, H. Sasaki, J. Nabekura, M. Sakaguchi, and K. Mihara. 2004. Membrane-embedded C-terminal segment of rat mitochondrial TOM40 constitutes protein-conducting pore with enriched beta-structure. *J. Biol. Chem.* 279:50619–50629.
20. Henry, J. P., P. Juin, F. Vallette, and M. Thieffry. 1996. Characterization and function of the mitochondrial outer membrane peptide-sensitive channel. *J. Bioenerg. Biomembr.* 28:101–108.
21. Fèvre, F., J. P. Henry, and M. Thieffry. 1994. Reversible and irreversible effects of basic peptides on the mitochondrial cationic channel. *Biophys. J.* 66:1887–1894.
22. Fèvre, F., J. P. Henry, and M. Thieffry. 1993. Solubilization and reconstitution of the mitochondrial peptide-sensitive channel. *J. Bioenerg. Biomembr.* 25:55–60.
23. Thieffry, M., J. Neyton, M. Pelleschi, F. Fevre, and J. P. Henry. 1992. Properties of the mitochondrial peptide-sensitive cationic channel studied in planar bilayers and patches of giant liposomes. *Biophys. J.* 63:333–339.
24. Chich, J. F., D. Goldschmidt, M. Thieffry, and J. P. Henry. 1991. A peptide-sensitive channel of large conductance is localized on mitochondrial outer membrane. *Eur. J. Biochem.* 196:29–35.
25. Juin, P., M. Thieffry, J. P. Henry, and F. M. Vallette. 1997. Relationship between the peptide-sensitive channel and the mitochondrial outer membrane protein translocation machinery. *J. Biol. Chem.* 272:6044–6050.
26. Künkele, K. P., P. Juin, C. Pompa, F. E. Nargang, J. P. Henry, W. Neupert, R. Lill, and M. Thieffry. 1998. The isolated complex of the translocase of the outer membrane of mitochondria. Characterization of the cation-selective and voltage-gated preprotein-conducting pore. *J. Biol. Chem.* 273:31032–31039.
27. Simon, S. M., and G. Blobel. 1991. A protein-conducting channel in the endoplasmic reticulum. *Cell.* 65:371–380.
28. Simon, S. M., and G. Blobel. 1992. Signal peptides open protein-conducting channels in E. coli. *Cell.* 69:677–684.
29. Hinnah, S. C., K. Hill, R. Wagner, T. Schlicher, and J. Soll. 1997. Reconstitution of a chloroplast protein import channel. *EMBO J.* 16:7351–7360.
30. Muro, C., S. M. Grigoriev, D. Pietkiewicz, K. W. Kinnally, and M. L. Campo. 2003. Comparison of the TIM and TOM channel activities of the mitochondrial protein import complexes. *Biophys. J.* 84:2981–2989.
31. Truscott, K. N., P. Kovermann, A. Geissler, A. Merlin, M. Meijer, A. J. Driessen, J. Rassow, N. Pfanner, and R. Wagner. 2001. A presequence- and voltage-sensitive channel of the mitochondrial preprotein translocase formed by Tim23. *Nat. Struct. Biol.* 8:1074–1082.
32. Kovermann, P., K. N. Truscott, B. Guiard, P. Rehling, N. B. Sepuri, H. Muller, R. E. Jensen, R. Wagner, and N. Pfanner. 2002. Tim22, the essential core of the mitochondrial protein insertion complex, forms a voltage-activated and signal-gated channel. *Mol. Cell.* 9:363–373.
33. Martinez-Caballero, S., S. M. Grigoriev, J. M. Herrmann, M. L. Campo, and K. W. Kinnally. 2007. Tim17p regulates the twin pore structure and voltage gating of the mitochondrial protein import complex TIM23. *J. Biol. Chem.* 282:3584–3593.
34. Meisinger, C., M. T. Ryan, K. Hill, K. Model, J. H. Lim, A. Sickmann, H. Muller, H. E. Meyer, R. Wagner, and N. Pfanner. 2001. Protein import channel of the outer mitochondrial membrane: a highly stable Tom40-Tom22 core structure differentially interacts with preproteins, small tom proteins, and import receptors. *Mol. Cell. Biol.* 21:2337–2348.
35. Woodhull, A. M. 1973. Ionic blockage of sodium channels in nerve. *J. Gen. Physiol.* 62:324–353.
36. Hille, B. 1992. Ionic Channels of Excitable Membranes. 2nd ed. Sinauer Associates, Sunderland, MA.
37. Kasianowicz, J. J., E. Brandin, D. Branton, and D. W. Deamer. 1996. Characterization of individual polynucleotide molecules using a membrane channel. *Proc. Natl. Acad. Sci. USA.* 93:13770–13773.
38. Akeson, M., D. Branton, J. Kasianowicz, E. Brandin, and D. Deamer. 1999. Microsecond time-scale discrimination among polycytidylic acid, polyadenylic acid, and polyuridylic acid as homopolymers or as segments within single RNA molecules. *Biophys. J.* 77:3227–3233.

39. Meller, A., L. Nivon, E. Brandin, J. Golovchenko, and D. Branton. 2000. Rapid nanopore discrimination between single polynucleotide molecules. *Proc. Natl. Acad. Sci. USA.* 97:1079–1084.
40. Vercoutere, W., S. Winters-Hilt, H. Olsen, D. Deamer, D. Haussler, and M. Akeson. 2001. Rapid discrimination among individual DNA molecules at single nucleotide resolution using a nanopore instrument. *Nat. Biotechnol.* 19:248–250.
41. Movileanu, L., J. P. Schmittschmitt, J. M. Scholtz, and H. Bayley. 2005. Interactions of peptides with a protein pore. *Biophys. J.* 89:1030–1045.
42. Bezrukov, S. M., I. Vodyanoy, and V. A. Parsegian. 1994. Counting polymers moving through a single ion channel. *Nature.* 370:279–281.
43. Meller, A. 2003. Dynamics of polynucleotide transport through nanometerscale pores. *J. Phys. Condens. Matter.* 15:R581–R607.
44. Ahting, U., C. Thun, R. Hegerl, D. Typke, F. E. Nargang, W. Neupert, and S. Nussberger. 1999. The TOM core complex: The general protein import pore of the outer membrane of mitochondria. *J. Cell Biol.* 147:959–968.
45. Benz, R., K. Janko, W. Boos, and P. Läuger. 1978. Formation of large, ion-permeable membrane channels by the matrix protein (porin) of Escherichia coli. *Biochim. Biophys. Acta.* 511:305–319.
46. Arnold, T., M. Poynor, S. Nussberger, A. N. Lupas, and D. Linke. 2007. Gene duplication of the eight-stranded β-barrel OmpX produces a functional pore: a scenario for the evolution of transmembrane β-barrels. *J. Mol. Biol.* 366:1174–1184.
47. Hanke, W., and W.-R. Schlue. 1993. Planar Lipid Bilayers. D. B. Satelle, editor. Academic Press, San Diego. 133 p.
48. Cooper, K., E. Jakobsson, and P. Wolynes. 1985. The theory of ion transport through membrane channels. *Prog. Biophys. Mol. Biol.* 46: 51–96.
49. Hall, J. E., C. A. Mead, and G. Szabo. 1973. A barrier model for current flow in lipid membranes. *J. Membr. Biol.* 11:75–97.
50. Patlak, J. B. 1993. Measuring kinetics of complex single ion channel data using mean-variance histograms. *Biophys. J.* 65:29–42.
51. Patlak, J. B. 1988. Sodium channel subconductance levels measured with a new variance-mean analysis. *J. Gen. Physiol.* 92:413–430.
52. VanDongen, A. M. J. 1996. A new algorithm for idealizing single ion channel data containing multiple unknown conductance levels. *Biophys. J.* 70:1303–1315.
53. VanDongen, A. M. J. 2004. Idealization and simulation of single ion channel data. *Methods Enzymol.* 383:229–244.
54. Sigworth, F. J., and S. M. Sine. 1987. Data transformations for improved display and fitting of single-channel dwell-time histograms. *Biophys. J.* 52:1047–1054.
55. Colquhoun, D., and F. J. Sigworth. 1983. Fitting and statistical analysis of single-channel records. *In* Single-Channel Recording, 1st ed. B. Sakmann and E. Neher, editors. Plenum Press, New York. 191–263.
56. Qin, F., A. Auerbach, and F. Sachs. 2000. A direct optimization approach to hidden Markov modeling for single channel kinetics. *Biophys. J.* 79:1915–1927.
57. Qin, F., A. Auerbach, and F. Sachs. 2000. Hidden Markov modeling for single channel kinetics with filtering and correlated noise. *Biophys. J.* 79:1928–1944.
58. Lohret, T. A., and K. W. Kinnally. 1995. Targeting peptides transiently block a mitochondrial channel. *J. Biol. Chem.* 270:15950–15953.
59. Henry, J. P., J. F. Chich, D. Goldschmidt, and M. Thieffry. 1989. Blockade of a mitochondrial cationic channel by an addressing peptide: an electrophysiological study. *J. Membr. Biol.* 112:139–147.
60. Winters-Hilt, S., W. Vercoutere, V. DeGuzman, D. Deamer, M. Akeson, and D. Haussler. 2003. Highly Accurate Classification of Watson-Crick Base-Pairs on Termini of Single DNA Molecules. *Biophys. J.* 84:967–976.
61. Meller, A., L. Nivon, and D. Branton. 2001. Voltage-driven DNA translocations through a nanopore. *Phys. Rev. Lett.* 6:3435–3438.
62. Henrickson, S., M. Misakian, B. Robertson, and J. Kasianowicz. 2000. Driven DNA transport into an asymmetric nanometer-scale pore. *Phys. Rev. Lett.* 85:3057–3060.
63. Babini, E., and M. Pusch. 2004. A two-holed story: structural secrets about ClC proteins become unraveled? *Physiology (Bethesda).* 19:293–299.
64. Miller, C. 1982. Open-state substructure of single chloride channels from Torpedo electroplax. *Philos. Trans. R. Soc. Lond. B Biol. Sci.* 299:401–411.
65. Adcock, C., G. R. Smith, and M. S. Sansom. 1998. Electrostatics and the ion selectivity of ligand-gated channels. *Biophys. J.* 75:1211–1222.
66. Pelleschi, M., J. P. Henry, and M. Thieffry. 1997. Inactivation of the peptide-sensitive channel from the yeast mitochondrial outer membrane: properties, sensitivity to trypsin and modulation by a basic peptide. *J. Membr. Biol.* 156:37–44.